



Published in final edited form as:

IEEE Trans Biomed Eng. 2008 November ; 55(11): 2584–2592. doi:10.1109/TBME.2008.2001284.

Prostate Cryotherapy Monitoring Using Vibroacoustography: Preliminary Results of an *Ex Vivo* Study and Technical Feasibility

Farid G. Mitri [Member, IEEE],

Department of Physiology and Biomedical Engineering, Ultrasound Research Laboratory, Mayo Clinic, Rochester, MN 55905 USA (mitri.farid@mayo.edu).

Brian J. Davis,

Department of Radiation Oncology, Mayo Clinic, Rochester, MN 55905 USA.

Azra Alizad,

Department of Physiology and Biomedical Engineering, Ultrasound Research Laboratory, Mayo Clinic, Rochester, MN 55905 USA.

James F. Greenleaf [Fellow, IEEE],

Department of Physiology and Biomedical Engineering, Ultrasound Research Laboratory, Mayo Clinic, Rochester, MN 55905 USA.

Torrence M. Wilson,

Department of Urology, Mayo Clinic, Rochester, MN 55905 USA.

Lance A. Mynderse, and

Department of Urology, Mayo Clinic, Rochester, MN 55905 USA.

Mostafa Fatemi [Senior Member, IEEE]

Department of Physiology and Biomedical Engineering, Ultrasound Research Laboratory, Mayo Clinic, Rochester, MN 55905 USA.

Abstract

The objective of this research is to prospectively evaluate the feasibility of vibroacoustography (VA) imaging in monitoring prostate cryotherapy in an *ex vivo* model. Baseline scanning of an excised human prostate is accomplished by a VA system apparatus in a tank of degassed water. Alcohol and dry ice mixture are used to freeze two prostate tissue samples. The frozen prostates are subsequently placed within the water tank at 27°C and rescanned. VA images were acquired at prescribed time intervals to characterize the acoustic properties of the partially frozen tissue. The frozen prostate tissue appears in the images as hypoemitting signal. Once the tissue thaws, previously frozen regions show coarser texture than prior to freezing. The margin of the frozen tissue is delineated with a well-defined rim. The thawed cryolesions show a different contrast compared with normal unfrozen prostate. In conclusion, this pilot study shows that VA produces clear images of a frozen prostate at different temperature stages. The frozen tissue appears as a uniform region with well-defined borders that are readily identified. These characteristic images should allow safer and more efficient application of prostatic cryosurgery. These results provide substantial motivation to further investigate VA as a potential modality to monitor prostate cryotherapy intraoperatively.

Keywords

Cryosurgery; prostate cancer; ultrasound; vibroacoustography (VA)

I. Introduction

PROSTATE cancer is recognized as one of the most prevalent malignant diseases and is the most commonly diagnosed cancer among men in the United States. In 2008, an estimated 186 320 men will be diagnosed with prostate cancer and 28 660 men will die of this disease [1]. Two forms of therapy for treating patients with localized prostate cancer are surgery [2] and radiation therapy [3]. Both therapies have undergone significant technical developments during the last ten years and can be delivered in various ways. However, both forms of established therapies have been related to significant complications and risks [3]. Because of the limitations of current therapies, there has been a continuous search for alternative procedures, such as cryosurgery, with the aim to cure prostate cancer [4].

In the mid nineteenth century, Arnott described the benefits of applying low temperatures for the therapeutic treatment of cancer [5]. During the mid 1960s, prostatic cryosurgery was the subject of important investigations [5]. However, complications due to an inability to adequately control the freezing process and the lack of proper equipment to protect both urethra and rectal wall limited its applicability. In the early 1990s, cryosurgery of the prostate was reintroduced clinically [6]–[19] due to improved ultrasound [11], [20], [21], MRI guidance [22]–[25], and cryotechnology [26]. Focal cryotherapy is gaining acceptance as an alternative that minimizes the side effects of standard therapy [27].

The new generation of cryotherapy (based on an advanced gas expansion method) uses argon and helium gases, which are delivered via cryoprobes (ranging in size from 1.5 to 3.4 mm diameter). A template similar to the one used for permanent seed implantation in brachytherapy [28], [29] is often used to guide cryoprobe placement. The treatment is performed under transrectal ultrasound (TRUS) guidance [7], [8], [21], and a urethral warming device is used together with thermocouples to better monitor and control the freezing process. However, the unipositional imaging (i.e., the prostate is only seen from the rectum side) presents an inconvenience because it only allows monitoring the ice growth from its posterior edge, while the anterior is in shadow. Computed tomography (CT) and MRI have prominent imaging advantages by circumferential visualization of the ice margins; however, they are expensive and somehow inconvenient to use for guidance, especially for the prostate gland.

With critical need to control the size, shape, and freeze–thaw characteristics of the iceball, efforts have been directed toward the use of real-time image-guided technologies to monitor treatment [30]–[32]. Failure to accurately monitor and modulate freezing in real time can lead to insufficient or excessive freezing and recurrence of malignancies or destruction of healthy tissues. Although investigators have reported the successful real-time monitoring of prostate cryosurgery with TRUS [7], [8], [11], [12], [21], there are drawbacks to this technique. Ultrasound imaging inherently produces a speckle, which is the snowy pattern that results from random interference of echoes from the tissue scatter. This artifact reduces image contrast, degrades its quality, and hampers accurate monitoring of cryolesions. Moreover, TRUS is not capable of distinguishing the subtleties of modulus of elasticity (variation of stiffness), and consequently, the ice–tissue interface is not well delineated. Additionally, TRUS cannot directly image even the gross differences in the temperature.

Recent breakthroughs in imaging have catalyzed the development of novel techniques, such as “elasticity imaging methods” that are sensitive to the elastic properties of tissue [33]–[35].

Among these techniques, a technique based on the dynamic radiation force of ultrasound developed at Mayo Clinic and known as VA [36], [37] has shown excellent capabilities in imaging tissues with variable stiffness values making it an ideal tool for detecting stiff inclusions within the tissue. Examples of such applications include detection of breast mass lesions and microcalcifications [38]–[41], mass lesions in excised human liver [42], and permanent brachytherapy metallic seeds [43] in an excised human prostate [44]. The feature of this technique versus conventional ultrasound is its insensitivity to object orientation [45], its speckle-free mode, and its high sensitivity to variations of tissue stiffness. The aim of this initial study is to introduce VA as an innovative image-guiding tool for cryotherapy monitoring and an alternative technique to TRUS. We present preliminary results showing the feasibility of using the VA technique to monitor prostate cryolesions.

II. Materials and Methods

A. VA Method and Experimental Setup

The VA imaging technique produces a map of the mechanical response of an object to a dynamic force applied to the object. The technique uses the radiation force of ultrasound to exert an oscillating stress field, localized in space. This force vibrates the object, which, in turn, produces a sound field in the medium. This sound field is received by an audio hydrophone placed near the object. The acoustic emission, which is normally in the low kilohertz range, is a function of the viscoelastic properties of the object and can be used to produce an image of the object. To confine the oscillating radiation stress to the desired region, VA uses two ultrasound beams driven at slightly different frequencies, propagating along separate paths. The beams are arranged to cross each other at their respective foci and thus produce a modulated field at a confined, small cross-sectional region. The radiation force resulting from mixing two ultrasound beams operating at different frequencies and intersecting in space is a nonlinear phenomenon in which multiple other frequencies are produced. One such frequency is a “difference frequency,” which represents a subtraction of the two operating frequencies. The object to be imaged is placed at the joint focal plane of the transducer elements, also known as the scanning plane. The ultrasound field produces a localized radiation stress field at the mutual focal point. Depending on the elastic properties of the object, the radiation tapping force may cause a portion of the object, or the entire object, to vibrate at this frequency. The acoustic emission resulting from object vibration is received by a hydrophone located nearby. Generally, the acoustic emission pressure field is almost omnidirectional. Therefore, at low frequencies, the hydrophone position is not a critical parameter in the measurement of the acoustic emission signal. To form an image, the focal point of the transducer is moved across the scanning plane on the object in a point-by-point raster pattern. The acoustic emission is received at each point, and an image is formed by displaying the magnitude (or phase) of such signals at corresponding positions on the image plane. The spatial resolution of this imaging method is determined by the ultrasound beam width at the focal plane, which is normally of the order of the incident ultrasound wavelength.

The VA imaging system apparatus used to scan the excised prostate is shown in Fig. 1. Two ultrasound beams were generated by a two-element homemade confocal transducer with a diameter of 45 mm, focal distance of 70 mm, and a center frequency of 3 MHz. The elements were driven by two tone-burst signals at frequencies of 3 and 3 MHz + 50 kHz. The burst-emitted signals were 100 μ s long at a pulse-repetition frequency (PRF) of 100 Hz. Each tone burst is long enough to accommodate five cycles at 50 kHz. The driving RF signals were obtained from two stable function generators (HP 33120 A, Hewlett-Packard Company, Houston, TX). The transducer was mounted on a three-axes positioning system and immersed in a tank of degassed water to ensure good acoustic coupling. The two ultrasound beams interacted at the joint focal region producing an oscillatory radiation stress field beating at the

“difference frequency” of the incident ultrasound beams (i.e., 50 kHz). The radiation stress field is confined to an ellipsoidal volume with major and minor axes that define the spatial resolutions. Spatial resolutions were determined by the focal depth (major axis) of the transducer and the diameter of the central lobe (minor axis). For this system, the axial and lateral resolutions, defined as the focal spot at full width at half-maximum, were 10 and 0.7 mm, respectively. The focal spot resolutions were measured experimentally in a previous work [46]. As a result of the applied oscillatory stress, an acoustic emission field was generated in the prostate and surrounding water at the same “difference frequency” (i.e., 50 kHz). VA images are acoustic emission magnitude images obtained at 50 kHz in which stiff regions (those with a high elastic modulus) are well identified from the surrounding soft tissue. The acoustic emission pressure field was detected with a submerged hydrophone (Model ITC—6050 C, Santa Barbara, CA) placed at 5 cm from the prostate edge. The hydrophone has a sensitivity of -157 dB re 1 V/ μ Pa, and frequency response between 1 Hz and 60 kHz. The signal received was bandpass filtered and amplified (Stanford Research Systems, SR650, Sunnyvale, CA) to eliminate noise, then digitized by a 12-bits/sample digitizer (National Instruments VXI-1000, Austin, TX) at a higher rate than the Nyquist rate. The data were recorded on a computer.

B. Excised Prostate Glands and Scanning Procedure

A freshly excised human prostate was removed via conventional radical retropubic prostatectomy as performed by a urologic surgeon. The excised human prostate was embedded in a gelatin phantom made by using 300 Bloom gelatin powder (Sigma-Aldrich, St. Louis, MO) with a concentration of 10% by volume. A preservative of potassium sorbate (Sigma-Aldrich) was also added with a concentration of 10 g/L. An X-ray image was initially obtained to serve as a reference for qualitative image comparison (see Fig. 2). Images of the fresh unfrozen prostate specimen were obtained with the VA system apparatus (see Fig. 1) along with a commercial Ultrasonix RP system. A mixture of alcohol with dry ice was used to freeze the prostate cast in the gel block down to -74 °C as measured by a microcomputer thermometer (Omega Engineering, Model HH-72 T, Stamford, CT) placed within the mixture. The frozen prostate was subsequently placed within the water tank 27 °C and VA images were acquired immediately after freezing and at 4-, 8-, 12-, 16-, 60-, and 120-min intervals as the frozen portion of the prostate thawed. At the same time, conventional ultrasound images were acquired at the end of each VA scan using the commercial Ultrasonix RP system. The VA images were acquired by scanning the transducer over the gland surface while recording the resulting acoustic emission pressure field. The images covered an area of 60 mm \times 60 mm, scanned at 0.25 mm/pixel incremental steps. The scanning time was 4 min for each VA scan.

To demonstrate the reproducibility and the VA appearance of frozen prostate tissue, VA experiments were conducted for a second prostate excised from a human cadaver. This prostate was initially placed in a saline solution bag and baseline scans performed within 2 h after excision. The images covered an area of 60 mm \times 80 mm, scanned at 0.25 mm/pixel incremental steps. The procedure is similar to the one described earlier, except only a portion of the prostate was frozen.

III. Results

Fig. 3 shows eight VA images at different time intervals: prior to freezing (a); immediately after freezing (b); 4 min after freezing (c); 8 min after freezing (d); 12 min after freezing (e); 16 min after freezing (f); 60 min after freezing (g); and 120 min after freezing at which time the prostate was completely thawed (h). The prostate is oriented in a way that the apex is located at the top of the figure.

The VA image obtained prior to freezing [see Fig. 3(a)] shows the prostate texture as well as bright dots that correspond to intraprostatic calcifications in clusters as confirmed by the X-

ray image (see Fig. 2). Immediately after freezing, the prostate frozen part [see Fig. 3(b)] shows a hypoemitting (dark) region with a well-defined “rim” at the edge (left side). The hypoemitting appearance of the frozen region may be described by two phenomena. In terms of a dynamic mechanical analysis, the frozen region has an increased stiffness and acts as a rigid immovable solid. When radiation force is applied to image the frozen tissue, its entire structure does not respond to the vibrating force as readily as the unfrozen regions of unchanged stiffness, and therefore, the frozen part appears as hyposignal in the VA image. Intraprostatic calcifications reappear in the image in addition to bright spots that might be small icy “islands” [see Fig. 3(d)]. As the frozen tissue continues thawing [see Fig. 3(e)], the cryolesions markedly showed different contrast compared with normal unfrozen prostate. At the end of the freezing process, the small icy “islands” completely disappear and the bright spots [see Fig. 3(f)–(h)] show the intraprostatic calcifications as confirmed by the X-ray (see Fig. 2). As noted, a different contrast has been observed in thawed tissue [see Fig. 3(f)–(h)] as compared to the VA image of the prostate prior to freezing [see Fig. 3(a)]. The acoustic impedance mismatch at the frozen–unfrozen tissue interface increases during the freezing process. This blocks the penetration of the primary ultrasound beams into the frozen region of the prostate and therefore reduces the VA signal. Therefore, the frozen part appears as dark regions in the VA image.

Fig. 4 shows eight conventional B-scan images obtained immediately after performing each VA scan. The images were obtained using a linear array transducer operating at 6.6 MHz and covered an area of 50 mm × 40 mm. Visual comparison of Figs. 3 and 4 reveals that VA produces clear images with a well-defined border of the ice ball as well as the boundaries of the frozen prostate. Moreover, the conventional B-mode images have a significant speckle that results in fuzzy borders that are hard to delineate at the frozen–unfrozen tissue interface, whereas VA images are free of speckle and produce clear and sharp borders.

Fig. 5 shows seven VA images of the second prostate at $\Delta f = 50$ kHz (a) prior to freezing; (b) immediately after freezing; (c) 4 min after freezing; (d) 10 min after freezing; (e) 16 min after freezing; (f) 60 min after freezing; and (g) 120 min after freezing at which time the prostate was completely thawed. In Fig. 5(a), two calcifications, one at upper center and other at lower left, appear as bright dots in the image. In Fig. 5(b), only the calcification at the lower left appears as a bright dot in the lower side of the image. The dark triangular region in the upper middle part of the image corresponds to the frozen portion of the prostate. The frozen region has masked the calcification at the upper center. In Fig. 5(c), the dark region in the upper half side of the prostate is reduced in size as compared with the one shown in Fig. 5(b) as the frozen part of the prostate is thawing. The margin of the frozen tissue appeared with a well-defined oval rim. The calcification at the upper center reappears as it is now outside the frozen region. In addition to the calcifications, other isolated bright spots appear that are believed to be ice patches randomly distributed within and around the frozen tissue. In Fig. 5(d), the frozen region in the upper half side of the prostate is mostly thawed as seen in this image. The calcifications as well as some small icy regions still appear as bright spots in the image. In Fig. 5(e), the small icy patches start to disappear as time passes. However, calcifications observed prior to freezing [seen in Fig. 5(a)] remain well displayed in the image. In Fig. 5(f), the small icy patches continue to disappear as time passes, but the calcifications remain visible in the image. In Fig. 5(g), the small icy patches are completely disappeared; the bright spots show the same intraprostatic calcifications that were seen in Fig. 5(a) prior to freezing. Notably, once the tissue thaws, previously frozen regions show coarser texture and appear darker than prior to freezing Fig. 5(a), which may be due to structural changes of tissue caused by freeze–thaw process.

IV. Discussion

In this research, we have performed an initial study of imaging a frozen prostate by VA. VA imaging of prostate with frozen parts offers a unique advantage compared to the conventional

ultrasound. VA images are sensitive to tissue stiffness and have no speckle. The results presented here are consistent with those previously obtained in detecting stiff inclusions within biological tissue [47], and provide encouraging data for further evaluation of VA as a means of monitoring prostate cryosurgery treatment.

Upon visual inspection of the VA images obtained at several freezing stages, it is quite noticeable that frozen parts are clearly identified from thawed prostate tissue. In addition, intraprostatic calcifications are clearly displayed, and can be identified from frozen regions as thawing time increases; calcifications consistently appear as bright spots in the VA images.

As discussed in Section II, the lateral spatial resolution for the 3 MHz ultrasound transducer is 0.7 mm (or 700 μm). In practice, TRUS is conventionally performed using a 5.0–7.5 MHz ultrasound frequency probe. Using a 5.0 MHz transducer, the lateral spatial resolution, defined by the focal beam width, would improve to around 0.5 mm compared to 0.7 mm of the present system. Therefore, one may anticipate better image quality by using higher ultrasound frequencies.

A critical point to consider is related to the acoustic shadowing that limits the ability of VA to identify the full extent of the ice ball within the prostate. As prostate tissue is frozen, the acoustic impedance mismatch increases, and therefore, ultrasound waves are reflected by the ice ball. This effect results in blocking the penetration of the primary ultrasound beams through the frozen region of the prostate, and therefore, reduces the VA signal from inside and beyond the frozen ice ball. As a result, the shadow caused by the ice may be greater in size than the ice ball itself. A similar problem also exists with conventional TRUS [7], [8], [12], [20], [21], [31]. One may mitigate this problem by using a specific transurethral VA probe that allows imaging the frozen prostate from the urethral side. This probe would be a modified version of the transurethral ultrasonography (TUUS) probe that has been used in clinical practice [48]. Further development of a transurethral VA (TUVA) probe and advanced investigation on its efficiency and practical use are warranted.

Another limitation is the result of two effects: phase aberration and sound speed variations in tissue. First, the ultrasound beams tend to defocus; second, the two beams may fail to intersect at their mutual focal point. The first effect results in beam broadening, which, in turn, results in the loss of spatial resolution and decreased sensitivity due to decreased peak radiation intensity. The second effect results in similar outcomes. In addition, this effect may cause the beams to intersect at an unanticipated location in the object and hence introduce image distortion. In this study, however, VA has shown high capability to delineate clearly frozen–soft boundaries. Therefore, these effects are expected to have a minor influence on the VA images.

Biological noise, such as respiration and cardiovascular system noise, is normally concentrated below the 1 kHz range, and is not expected to interfere with the reception of the acoustic emission signal.

In this study, images of the frozen prostate are obtained only in two dimensions (i.e., a single slice). However, the ultrasound beam used here produces a stress field that is confined in three dimensions. Therefore, it is possible, in principle, to selectively scan several slices of the object at different depths to produce a 3-D (volume) image of the object. It is noted that for clinical applications, ultrasound attenuation is strongly depth-dependent. Tissue attenuation reduces the ultrasound intensity of the primary beams and hence the low-frequency acoustic emission signal. Attenuation also limits the usable ultrasound frequency, thus lowering resolution. Further research must concentrate on 3-D VA to improve its performance.

The scanning mechanism used for this experiment is a relatively lengthy process (around 4 min to achieve the scan). A long imaging time is not desirable for prostate imaging because body motions within this period can introduce “motion artifact” in the images and the procedure anesthesia time could be impractical. Besides, proper monitoring of cryotherapy requires faster imaging. One way to reduce the scanning time significantly is to use electronic focusing [49]. Current research in our group is directed toward the development and testing of a linear array probe with dynamic focusing whereby the imaging time should be reduced to less than a minute for an 80 mm × 60 mm scanning area.

Although VA uses ultrasound as a noninvasive energy source, the system properties are different from those of conventional pulse-echo ultrasound imaging (B-scan), and in particular, TRUS. As a result, VA promises new diagnostic applications not normally offered by the conventional ultrasound. A notable advantage of VA over TRUS is that VA can image prostate frozen parts boundaries with no speckles, which is of an important clinical value. A major distinction between VA and B-mode ultrasound stems from the fact that VA is sensitive to the mechanical properties of the object at low frequencies (the difference frequency Δf), whereas ultrasound B-mode imaging is only sensitive to properties of the medium at much higher ultrasound frequencies. B-mode ultrasound is only sensitive to the local properties of the object (such as the ultrasound reflection coefficient) at the focal point. In VA, the acoustic emission is a function of: 1) local properties and 2) global properties of the object [36]. The local properties determine how much radiation force is generated on the object. The global properties define how the object responds to the radiation force as a vibrating structure. Frozen and thawed tissues have different mechanical properties (stiffness and damping). Therefore, their response to the vibrating force is not the same. This may explain why frozen and thawed parts are differentiated in a VA image. This is a unique capability of VA not available from other imaging modalities such as conventional ultrasound.

The focus of this study was to assess the capability of VA in identifying frozen parts in a human noncancerous prostate specimen. Cancerous prostatic tissue, as well as healthy prostatic tissue, may contain firm inclusions. Once detected by the VA system, hard lesions may be therefore confused with frozen tissue. However, after tissue thaws, it is anticipated that hard lesions will remain detectable in the VA image. In this initial feasibility study, no attempt has been made to study cancerous prostates. Further investigation is required to address this issue.

A key question is whether VA can function properly *in vivo*. To answer this question, we refer to previous work on breast imaging with VA [41], [47]. In these papers, it was shown that VA could produce high-quality images of human breast at ultrasound intensities within the limits defined by the FDA for diagnostic ultrasound. These results provide impetus to design a specific system for *in vivo* prostate cryotherapy monitoring, which includes all the integrated components as shown in Fig. 6.

V. Conclusion

In summary, VA is introduced for monitoring prostate cryotherapy and as an alternative to other existing techniques. The feature of this method is its speckle-free high-resolution images (uncommon with conventional ultrasound), and its sensitivity to detect tissue stiffness and boundaries. VA experiments are conducted on excised frozen human prostates, and images are obtained at several time intervals as it thaws. Preliminary results of this experiment, conducted under well-controlled conditions in a water tank, indicate that VA is potentially an alternative and useful technique for monitoring prostate cryotherapy, providing clear images of the frozen tissue at different temperature stages. These results provide substantial motivation to further investigate VA as a modality to monitor prostate cryotherapy intraoperatively.

Acknowledgment

The authors would like to thank R. R. Kinnick and T.M. Kinter for technical and laboratory support. Disclosure of conflict of interest: Some of the techniques used here are patented by Mayo Clinic and some of the authors (JFG, MF).

This work was supported in part by the National Institute of Health under Grant EB 00535-04 and Grant CA 91956-06P2.

Biography



Farid G. Mitri (M'00) received the B.S. degree in physics from the Faculty of Sciences II, Lebanese University, Beirut, Lebanon, in 2000, and the M.S. and Ph.D. degrees in biomedical

engineering (with highest honors and committee distinction) from the University Claude Bernard Lyon 1, Lyon, France, in 2001 and 2004, respectively.

He was awarded a fellowship from the City of Lyon, France, to continue his M.S. research studies at the Nuclear Magnetic Resonance Imaging Laboratory, Lyon, France. He was also awarded a fellowship from the National Institute of Health and Medical Research (INSERM), Lyon, to pursue his Ph.D. thesis at the Therapeutic Ultrasound Research Laboratory, Unit 556 of INSERM. In October 2004, he joined the Ultrasound Research Laboratory, Mayo Clinic, Rochester, MN, where he is currently an Assistant Professor of biomedical engineering. His current research interests include ultrasonic biomedical imaging science as well as the theory and applications of the acoustic radiation force, acoustic scattering, and vibrations in biomedical applications.

Dr. Mitri is the recipient of the 2005 Lyon City Young Investigator Award, the 2007 Edward C. Kendall Award from Mayo Clinic, as well as seven travel awards for participation in international meetings. In September 2007, he was awarded the National Order of the Cedar at the Officer level, the highest civilian award in his native Lebanon. He is a member of the Institute of Electrical and Electronics Engineers (IEEE), the American Society of Mechanical Engineers (ASME), the Acoustical Society of America (ASA), the French Acoustical Society (SFA), Sigma Xi, and the Mayo Clinic Alumni Association.



Brian J. Davis received the B.S. degree in nuclear engineering from the University of Illinois, Urbana, in 1982, the M.S. and Ph.D. degrees in mechanical engineering from Massachusetts Institute of Technology (MIT), Cambridge, in 1984 and 1990, respectively, and the M.D. degree from the University of Illinois, Chicago, in 1992.

He was at the Harvard–MIT Laboratory of Biomedical Ultrasonics. During 1979–1980, he was a Munich Exchange Scholar at the Technical University of Munich. Since 1996, has been with the Mayo Clinic, Rochester, MN, where he is currently an Associate Professor of radiation oncology, and specializes in the radiotherapeutic management of prostate cancer. He is on leave-of-absence to run for the U.S. House of Representatives in the First District of Minnesota. He received a five-year M.D.–Ph.D. scholarship from the Life and Health Insurance Medical

Research Fund, the internship training at Evanston Hospital, a Northwestern University Program, Evanston, IL, and specialty training in radiation oncology in 1996 at Memorial Sloan Kettering Cancer Center.

Dr. Davis is the President of the American Brachytherapy Society for 2008–2009.



Azra Alizad received the M.D. degree from Tehran University of Medical Sciences, Tehran, Iran, in 1978.

She joined the faculty of Tehran University as an Assistant Professor of pediatrics. In 1994, she joined the University of Florida, Gainesville, as a Visiting Assistant Professor of pediatrics,

where she was engaged in ultrasound imaging research. She was engaged in echocardiography of genetic disorders in the Cardiovascular Division, Internal Medicine Department, Mayo Clinic, Rochester, MN, where, in 2001, she was with the Ultrasound Research Laboratory and is currently an Associate Professor of biophysics at the College of Medicine. She is also a member of the Mayo Cancer Center and Mayo Cancer Imaging Program. She is a Board Certified Pediatrician from Tehran University of Medical Sciences. Her current research interests include applications of ultrasound radiation force and low-frequency vibration in biomedicine, and *in vivo* vibroacoustography of breast, prostate, and thyroid. She has authored or coauthored a number of papers to the leading peer-reviewed journals.

Dr. Alizad is a member of the Sigma-Xi Society, the American Institute of Ultrasound in Medicine, and the American Cancer Society.



James F. Greenleaf (M'73–SM'84–F'88) was born in Salt Lake City, UT, on February 10, 1942. He received the B.S. degree in electrical engineering from the University of Utah, Salt Lake City, in 1964, the M.S. degree in engineering science from Purdue University, West Lafayette, IN, in 1968, and the Ph.D. degree in engineering science from the Mayo Graduate School of Medicine, Rochester, MN, and Purdue University, in 1970.

He is currently a Professor of biophysics and an Associate Professor of medicine at Mayo Graduate School, Rochester. He is also a Consultant in the Department of Physiology and Biomedical Engineering, and Internal Medicine, Division of Cardiovascular Diseases, Mayo Clinic Rochester, Rochester. His current research interests include ultrasonic biomedical science. He has authored or coauthored more than 327 articles and has edited five books. He holds twelve patents.

Prof. Greenleaf has been with the IEEE Technical Committee for the Ultrasonics Symposium for five years, and also the IEEE Ultrasonics, Ferroelectrics, and Frequency Control Society (UFFC-S) Subcommittee on Ultrasonics in Medicine/IEEE Measurement Guide Editors, and the IEEE Medical Ultrasound Committee. In 1992 and 1993, he was the President of the UFFC-S, where he is currently the Vice President for Ultrasonics. He was the Distinguished Lecturer for the IEEE Ultrasonics, Ferroelectrics, and Frequency Control Society, during 1990–1991. He was the recipient of the 1986 J. Holmes Pioneer Award, the 1998 William J. Fry Memorial Lecture Award from the American Institute of Ultrasound in Medicine, the 2003 Achievement Award, the 2004 Rayleigh Award, and the 2007 Distinguished Service Award of the IEEE-Ultrasonics, Ferroelectrics, and Frequencies Control Society (UFFC-S). He is a Fellow of the American Institute of Ultrasound in Medicine and the American Institute for Medical and Biological Engineering.



Torrence M. Wilson received the B.S. degree from The United States Military Academy at West Point, New York, in 1966 and the M.D. degree from the Medical College of Georgia, in 1974.

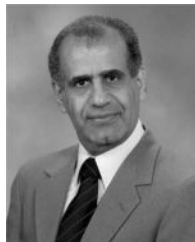
He completed urology residency in 1979 and is board certified by the American Board of Urology. He is a Consultant in the Department of Urology, Mayo Clinic, Rochester, MN. His current research interests include prostate cancer: prostate cancer prevention therapies, minimally invasive therapies including brachytherapy, cryosurgery, and HIFU, and for recurrent prostate cancer *in-situ* gene therapy; bladder cancer: localized surgical (including laser) and intravesical therapies, and HEXVIX florescent enhanced surgery; benign prostatic hypertrophy (BPH): invasive and minimally invasive therapies including lasers (greenlight and

holmium), stents, microwave, interstitial therapy (TUNA), and botox injection therapy; urologic imaging: trans urethral ultrasound applications for prostate biopsy, brachytherapy, and cryotherapy, 3-D ultrasound applications for prostate diagnosis and therapies, Ultrasound-MRI fusion applications for these procedures, MRI guided cryosurgery, and prostate imaging by vibro-acoustography; and urethral stricture therapies including stents.



Lance A. Mynderse received the B.S. degree in zoology from Duke University, Durham, NC, in 1974, the M.S. degree in pathology from Hahnemann University, Philadelphia, PA, in 1982, and the M.D. degree from Texas A&M University of the Health Sciences, College Station, in 1987.

In 1993, he completed his surgical internship and urological surgical training at Mayo Graduate School of Medicine, Rochester, MN. In 2000, he joined the Department of Urology, Mayo Clinic, Rochester. His current research interests include minimally invasive therapies for benign prostatic hyperplasia and prostate cancer. He is the Principal or Coinvestigator for more than 15 ongoing clinical trials, including the National Institute of Health (NIH) sponsored Minimally Invasive Surgical Treatment (MIST) Multicenter Trial for benign prostatic hyperplasia (BPH).



Mostafa Fatemi (S'75–M'78–SM'07) received the Ph.D. degree in electrical engineering from Purdue University, West Lafayette, IN, in 1979.

He is currently a Professor of biomedical engineering at Mayo Clinic College of Medicine, Rochester, MN, and a member of the Mayo Clinic Cancer Center, the Cancer Imaging Program, and the Prostate Cancer Program. His current research interests include ultrasound imaging and evaluation of the elastic properties of biological tissues by means of ultrasound radiation force. He leads research programs in the areas of breast and prostate imaging and tissue characterization. He has authored or coauthored over 100 peer-reviewed and proceedings papers, ten book chapters, and is the editor of a book entitled *Biomedical Applications of Vibration and Acoustics in Imaging and Characterization*. His pioneering work includes a novel imaging method known as vibroacoustography, which was presented in *Science* in 1998 and the *Proceedings of the National Academy of Sciences* in 1999. He also holds six patents on various aspects of vibroacoustography and auditory effects of ultrasound on fetus.

Dr. Fatemi has been on the Editorial Boards of a number of journals, including the IEEE TRANSACTIONS ON MEDICAL IMAGING. He is a Fellow of the American Institute for Medical and Biological Engineering.

REFERENCES

1. Jemal A, Siegel R, Ward E, Hao Y, Xu J, Murray T, Thun MJ. Cancer statistics, 2008. *CA Cancer J. Clin* 2008;58:71–96. [PubMed: 18287387]
2. Flocks RH, O'Donoghue EPN, Millemann LA, Culp DA. Surgery of prostate carcinoma. *Cancer* 1975;36:705–717. [PubMed: 1157032]
3. Garnick MB. Prostate-cancer—Screening, diagnosis, and management. *Ann. Internal Med* 1993;118:804–818. [PubMed: 7682387]
4. Gillett MD, Gettman MT, Zincke HT, Blute ML. Tissue ablation technologies for localized prostate cancer. *Mayo Clin. Proc* 2004;79:1547–1555. [PubMed: 15595340]
5. Gage AA. History of cryosurgery. *Seminars Surg. Oncol* 1998;14:99–109.
6. Loening S, Hawtrey C, Bonney W, Narayana A, Culp DA. Cryotherapy of prostate cancer. *Prostate* 1980;1:279–286. [PubMed: 7279801]
7. Onik GM, Cohen JK, Reyes GD, Rubinsky B, Chang ZH, Baust J. Transrectal ultrasound-guided percutaneous radical cryosurgical ablation of the prostate. *Cancer* 1993;72:1291–1299. [PubMed: 7687922]
8. Bahn D, Lee F, Solomon M, Gontina H, Klionsky D, Lee F Jr. Prostate cancer: US-guided percutaneous cryoablation. *Work in progress. Radiology* 1995;194:551–556. [PubMed: 7529937]
9. Littrup PJ, Sparschu RA, Grignon D. Prostate cryotherapy. *Cancer* 1995;75:1957–1962.
10. Falconieri G, Lugnani F, Zanconati F, Signoretto D, DiBonito L. Histopathology of the frozen prostate the microscopic bases of prostatic carcinoma cryoablation. *Pathol. Res. Practice* 1996;192:579–587.
11. Onik GM, Downey DB, Fenster A. Three-dimensional sonographically monitored cryosurgery in a prostate phantom. *J. Ultrasound Med* 1996;15:267–270. [PubMed: 8919513]
12. Wong W, Chinn D, Chinn M, Chinn J, Tom W, Tom W. Cryosurgery as a treatment for prostate carcinoma. *Cancer* 1997;79:963–974. [PubMed: 9041159]
13. Patel BG, Parsons CL, Bidair M, Schmidt JD. Cryoablation for carcinoma of the prostate. *J. Surg. Oncol* 1996;63:256–264. [PubMed: 8982371]
14. Schmidt JD, Doyle J, Larison S. Prostate cryoablation: Update 1998. *CA-A Cancer J. Clin* 1998;48:239–253.
15. Drachenberg D. Treatment of prostate cancer: Watchful, waiting, radical prostatectomy, and cryoablation. *Seminars Surg. Oncol* 2000;18:37–44.
16. Bahn DK, Lee F, Badalament R, Kumar A, Greski J, Chernick M. Targeted cryoablation of the prostate: 7-year outcomes in the primary treatment of prostate cancer. *Urology* 2002;60:3–11. [PubMed: 12206842]
17. Pareek G, Nakada SY. The current role of cryotherapy for renal and prostate tumors. *Urol. Oncol.-Seminars Original Invest* 2005;23:361–366.
18. Mouraviev V, Polascik TJ. Update on cryotherapy for prostate cancer in 2006. *Curr. Opin. Urol* 2006;16:152–156. [PubMed: 16679851]
19. Galosi AB, Lugnani F, Muzzonigro G. Reviews in endourology salvage cryosurgery for recurrent prostate carcinoma after radiotherapy. *J. Endourol* 2007;21:1–7. [PubMed: 17263599]
20. Onik G, Cobb C, Cohen J, Zabkar J, Porterfiled B. US characteristics of frozen prostate. *Radiology* 1988;168:629–631. [PubMed: 3043544]
21. Lee F, Bahn DK, McHugh TA, Onik GM, Lee FT. US-guided percutaneous cryoablation of prostate cancer. *Radiology* 1994;192:769–776. [PubMed: 8058945]
22. Rubinsky B, Gilbert JC, Onik GM, Roos MS, Wong STS, Brennan KM. Monitoring cryosurgery in the brain and in the prostate with proton NMR. *Cryobiology* 1993;30:191–199. [PubMed: 8319488]
23. Pease GR, Wong STS, Roos MS, Rubinsky B. MR image-guided control of cryosurgery. *J. Magn. Reson. Imag* 1995;5:753–760.
24. Kalbhen C, Hricak H, Shinohara K, Chen M, Parivar F, Kurhanewicz J, Vigneron D, Carroll P. Prostate carcinoma: MR imaging findings after cryosurgery. *Radiology* 1996;198:807–811. [PubMed: 8628875]

25. Vellet A, Saliken J, Donnelly B, Raber E, McLaughlin R, Wiseman D, Ali-Ridha N. Prostatic cryosurgery: Use of MR imaging in evaluation of success and technical modifications. *Radiology* 1997;203:653–659. [PubMed: 9169684]
26. Lee F, Bahn DK, Badalament RA, Kumar AB, Klionsky D, Onik GM, Chinn DO, Greene C. Cryosurgery for prostate cancer: Improved glandular ablation by use of 6 to 8 cryoprobes. *Urology* 1999;54:135–140. [PubMed: 10414740]
27. Bahn DK, Silverman P, Lee F, Badalament R, Bahn ED, Rewcastle JC. Focal prostate cryoablation: Initial results show cancer control and potency preservation. *J. Endourol* 2006;20:688–692. [PubMed: 16999628]
28. Syed AMN, Puthawala A, Sharma A, Gamie S, Londrc A, Cherlow JM, Damore SJ, Nazmy N, Sheikh KM, Ko SJ. High-dose-rate brachytherapy in the treatment of carcinoma of the prostate. *Cancer Control* 2001;8:511–521. [PubMed: 11807421]
29. Beyer DC. The evolving role of prostate brachytherapy. *Cancer Control* 2001;8:163–170. [PubMed: 11326171]
30. Rubinsky B. Cryosurgery. *Annu. Rev. Biomed. Eng* 2000;2:157–187. [PubMed: 11701510]
31. Onik G. Image-guided prostate cryosurgery: State of the art. *Cancer Control* 2001;8:522–531. [PubMed: 11807422]
32. Zou KH, Tuncali K, Warfield SK, Zentai CP, Worku D, Morrison PR, Silverman SG. Three-dimensional assessment of MR imaging-guided percutaneous cryotherapy using multi-performer repeated segmentations: The value of supervised learning. *Acad. Radiol* 2005;12:444–450. [PubMed: 15831417]
33. Greenleaf JF, Fatemi M, Insana MF. Selected methods for imaging elastic properties of biological tissues. *Annu. Rev. Biomed. Eng* 2003;5:57–78. [PubMed: 12704084]
34. Fatemi M, Manduca A, Greenleaf JF. Imaging elastic properties of biological tissues by low-frequency harmonic vibration. *Proc. IEEE Oct.;*2003 91(10):1503–1519.
35. Pellot-Barakat C, Sridhar M, Lindfors KK, Insana MF. Ultrasonic elasticity imaging as a tool for breast cancer diagnosis and research. *Curr. Med. Imag. Rev* 2006;2:157–164.
36. Fatemi M, Greenleaf JF. Ultrasound-stimulated vibro-acoustic spectrography. *Science* 1998;280:82–85. [PubMed: 9525861]
37. Fatemi M, Greenleaf JF. Vibro-acoustography: An imaging modality based on ultrasound-stimulated acoustic emission. *Proc. Nat. Acad. Sci. USA* 1999;96:6603–6608. [PubMed: 10359758]
38. Fatemi M, Wold LE, Alizad A, Greenleaf JF. Vibro-acoustic tissue mammography. *IEEE Trans. Med. Imag Jan.;*2002 21(1):1–8.
39. Alizad A, Fatemi M, Whaley DH, Greenleaf JF. Application of vibro-acoustography for detection of calcified arteries in breast tissue. *J. Ultrasound Med* 2004;23:267–273. [PubMed: 14992365]
40. Alizad A, Fatemi M, Wold LE, Greenleaf JF. Performance of vibro-acoustography in detecting microcalcifications in excised human breast tissue: A study of 74 tissue samples. *IEEE Trans. Med. Imag Mar.;*2004 23(3):307–312.
41. Alizad A, Whaley DH, Greenleaf JF, Fatemi M. Potential applications of vibro-acoustography in breast imaging. *Technol. Cancer Res. Treatment* 2005;4:151–157.
42. Alizad A, Wold LE, Greenleaf JF, Fatemi M. Imaging mass lesions by vibro-acoustography: Modeling and experiments. *IEEE Trans. Med. Imag Sep.;*2004 23(9):1087–1093.
43. Mitri FG, Trompette P, Chapelon JY. Improving the use of vibro-acoustography for brachytherapy metal seed imaging: A feasibility study. *IEEE Trans. Med. Imag Jan.;*2004 23(1):1–6.
44. Mitri FG, Davis BJ, Alizad A, Urban MW, Greenleaf JF, Kin-nick RR, Lischer GH, Wilson TM, Fatemi M. Vibroacoustography imaging of permanent brachytherapy seeds in an excised human prostate allows seed imaging independent of seed orientation. *Ultrasonics*. accepted for publication
45. Mitri FG, Davis BJ, Greenleaf JF, Fatemi M. Comparative study of vibro-acoustography versus pulse-echo ultrasound in imaging permanent prostate brachytherapy seeds. *Ultrasonics*. accepted for publication
46. Fatemi M, Greenleaf JF. Probing the dynamics of tissue at low frequencies with the radiation force of ultrasound. *Phys. Med. Biol* 2000;45:1449–1464. [PubMed: 10870703]

47. Alizad A, Whaley DH, Greenleaf JF, Fatemi M. Critical issues in breast imaging by vibro-acoustography. *Ultrasonics* 2006;44:217–220.
48. Nathan MS, Mei Q, Seenivasagam K, Davies B, Wickham JEA, Miller RA. Comparison of prostatic volume and dimensions by transrectal and transurethral ultrasonography. *Br. J. Urol* 1996;78:84–89. [PubMed: 8795406]
49. Silva GT, Greenleaf JF, Fatemi M. Linear arrays for vibro-acoustography: A numerical simulation study. *Ultrason. Imag* 2004;26:1–17.

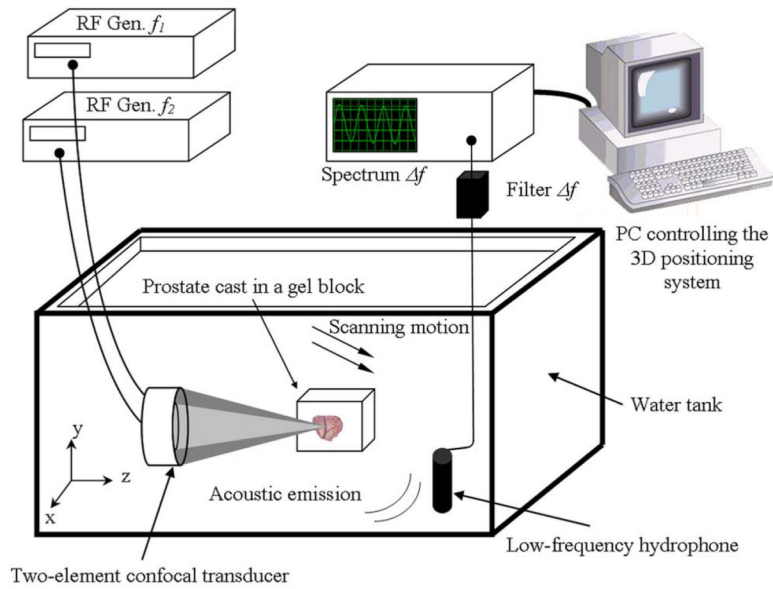


Fig. 1. Experimental VA system diagram. The excised prostate gland embedded in the gel was placed within a water tank at the focus of the confocal ultrasound transducer and scanned. The two ultrasound beams differ in frequency by Δf . The hydrophone receives the acoustic emission signal (at Δf) from the prostate. This signal is processed and mapped into an image.

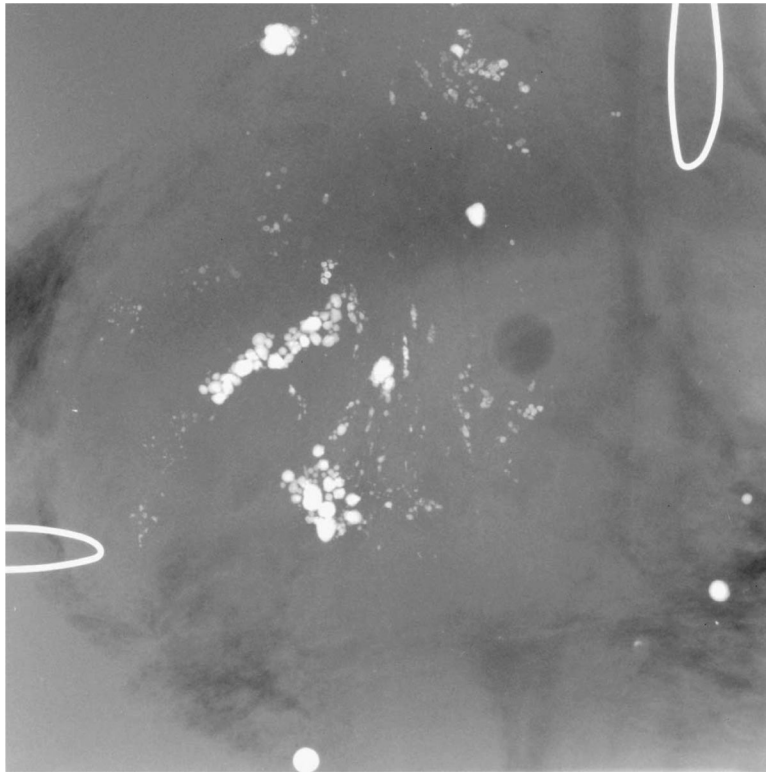


Fig. 2. X-ray image of the freshly excised prostate. The bright spots show the intraprostatic calcifications. Two wire loops (shown in the top right and lower left of the image) are used as registration markers in the X-ray system.

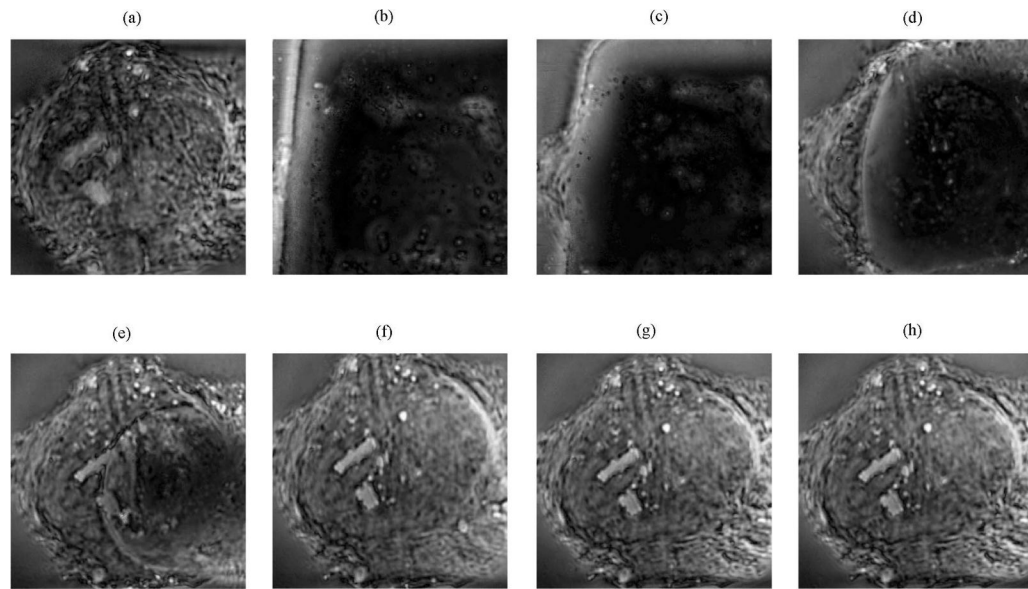


Fig. 3. Experimental VA image at $\Delta f = 50$ kHz of the excised prostate. (a) Prior to freezing. (b) Immediately after freezing. (c) 4 min after freezing. (d) 8 min after freezing. (e) 12 min after freezing. (f) 16 min after freezing. (g) 60 min after freezing. (h) 120 min after freezing so the prostate was completely thawed. In (a), intraprostatic calcifications in clusters appear as bright dots in the image. In (b), the dark region in the right part of the image corresponds to the frozen portion of the prostate as well as a part of the gel that was frozen during the freezing process. In (b) and (c), isolated bright spots other than the calcification are believed to be patches of ice randomly distributed within and around the frozen tissue. In (c) and (d), the dark region in the right side of the prostate image is reducing in size as compared with the one shown in (b) as the frozen part of the prostate is thawing. The margin of the frozen tissue appeared with a well-defined rim in (d) and (e). After 12 min, the frozen region of the prostate is mostly thawed as seen in (f) through (h). The calcifications in clusters appear as bright spots in the image.

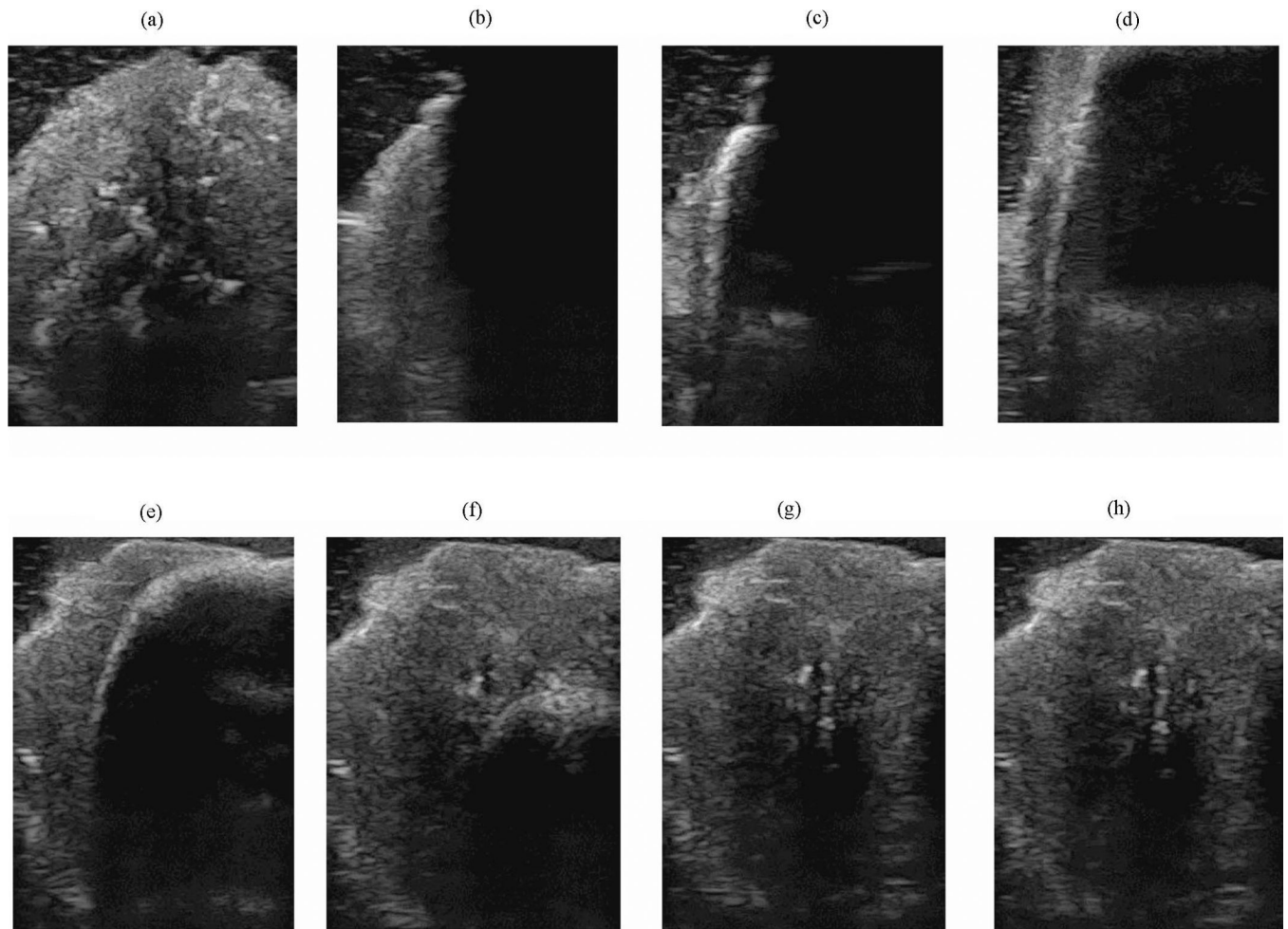


Fig. 4. Experimental B-scan ultrasound image at 6.6 MHz of the excised prostate. (a) Prior to freezing. (b) Immediately after freezing. (c) 4 min after freezing. (d) 8 min after freezing. (e) 12 min after freezing. (f) 16 min after freezing. (g) 60 min after freezing. (h) 120 min after freezing so the prostate was completely thawed. A portion of the gel block holding the tissue was frozen in the process. The border of frozen tissue is more prominent in (e).

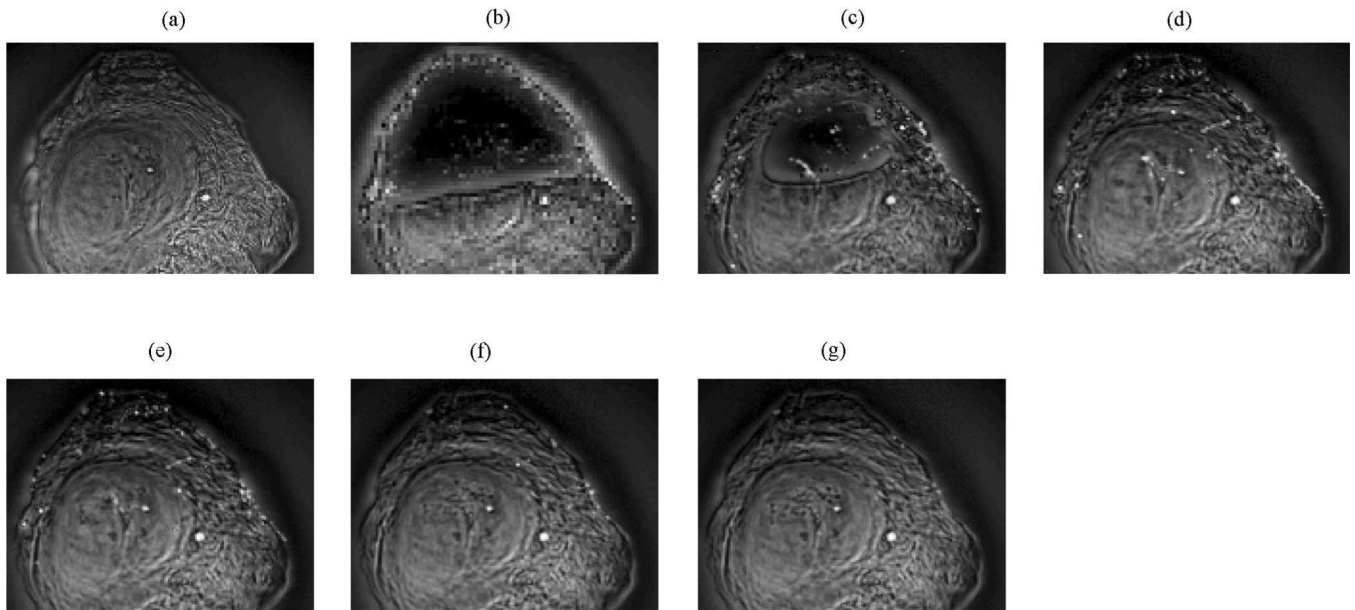


Fig. 5.

Experimental VA image of the second prostate at $\Delta f = 50$ kHz. (a) Prior to freezing. (b) Immediately after freezing. (c) 4 min after freezing. (d) 10 min after freezing. (e) 16 min after freezing. (f) 60 min after freezing. (g) 120 min after freezing so the prostate was completely thawed. In (a), two calcifications appear as bright dots in the image. In (b), one of the calcifications appears as a bright dot in the lower side of the image. The dark region in the upper middle part of the image corresponds to the frozen portion of the prostate. Isolated bright spots other than the calcification are believed to be patches of ice randomly distributed within and around the frozen tissue. These small isolated ice patches behave as calcifications as they appear as bright spots in the image. In (c), the calcifications that appeared prior to freezing (a) reappear. In addition, bright spots within the dark region in the image are believed to be small areas of ice. The dark region in the upper half side of the prostate is reduced in size as compared with the one shown in (b) as the frozen part of the prostate is thawing. The margin of the frozen tissue appeared with a well-defined rim. In (d), the frozen region in the upper half side of the prostate is mostly thawed as seen in this image. The calcifications reappear as bright spots in the image. In (e), the remaining dispersed bright spots that might be small icy patches, start to disappear as time passes. However, calcifications observed prior to freezing [seen in (a)] remain well displayed in the image. In (f), the small icy patches continue to disappear as time passes, but the calcifications remain visible in the image. In (g), the small icy patches are completely disappeared; the bright spots show the intraprostatic calcifications [seen in (a)] prior to freezing. Notably, once the tissue thaws, previously frozen regions show different texture and contrast than prior to freezing (a).

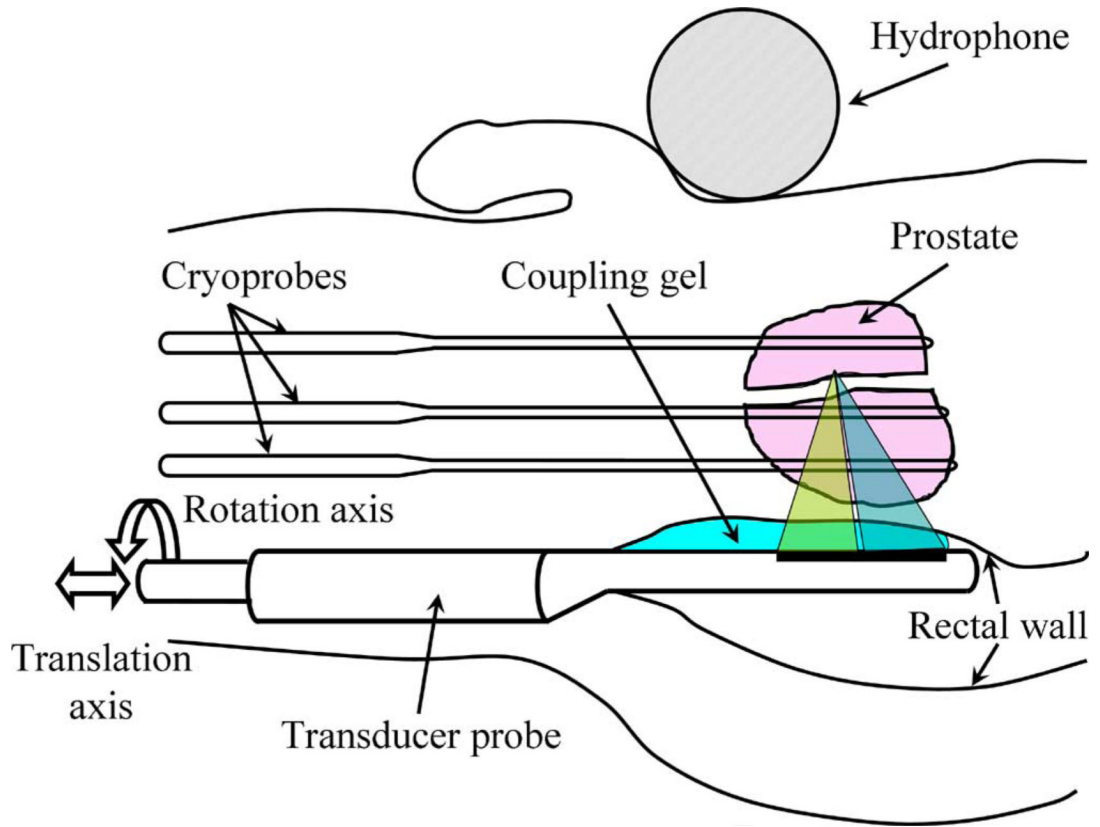


Fig. 6. Transrectal VA system including the transducer, hydrophone, and cryoprobes. Elements of the transducer are divided into two groups excited at f_1 and f_2 , respectively, to produce two beams at different frequencies focused at a common focal spot. The position of the hydrophone in this schematic is typical. However, the hydrophone can be placed at a different desired location near the prostate.